Nonlinear Dyn (2015) 79:1711–1726
DOI 10.1007/s11071-014-1769-3

ORIGINAL PAPER

Experimental and numerical investigation of friction element dissipative effects in blade shrouding

Luděk Pešek · Michal Hajžman · Ladislav Půst · Vladimír Zeman · Miroslav Byrtus · Jan Brůha

Received: 20 August 2012 / Accepted: 23 October 2014 / Published online: 6 November 2014

Abstract Friction forces can be advantageously used as a source of passive damping in various mechanical systems. This paper deals with an experimental modelling and numerical simulation of blades interaction by means of a friction element placed in the shroud between the blade heads. The radial force, which represents the centrifugal force acting on the friction element, determines the values of contact forces between the element and blades. The experimental set-up for a couple of non-rotating blades is described in the paper, and the measured dynamic response of two blades is documented. The same situation is modelled by means of a basic and a more complex dynamical model of two blades with a friction element. The effect of friction is studied for the case of harmonic excitation by suitable frequency and subsequent free vibration attenuation. Both mathematical models are based on the finite element method combined with lumped rigid bodies. The interaction of the friction element and blades is described by normal contact and tangential friction forces derived for particular geometrical parameters of the studied mechanical system. The performed comparison of experimental and numerical results shows the satisfactory agreement and the modelling methodology could be used for possible parameter optimization.

Keywords Vibrations · Turbine blades · Contact · Friction · Experimental measurement · Finite element method

L. Pešek · L. Půst
Institute of Thermomechanics, Academy of Sciences of the Czech Republic, Dolejškova 5, 182 00 Praha 8, Czech Republic
e-mail: pesek@it.cas.cz

L. Půst
e-mail: pust@it.cas.cz

M. Hajžman (✉) · V. Zeman · M. Byrtus · J. Brůha
Department of Mechanics, University of West Bohemia, Univerzitní 22, 306 14 Plzeň, Czech Republic
e-mail: mhajzman@kme.zcu.cz

V. Zeman
e-mail: zemanv@kme.zcu.cz

M. Byrtus
e-mail: mbyrtus@kme.zcu.cz

J. Brůha
e-mail: jbruha@students.zcu.cz

1 Introduction

Turbine blades are subjected to higher and higher static and dynamic straining with development of higher efficiency and power range of steam and gas turbines. Although the turbines and their bladings can be carefully designed, it is not possible to omit resonant vibration leading to a high-cycle fatigue risk. The resonance phenomena arise from two different mechanisms depending on whether it is forced response vibration or self-excited vibration. The former case leads to so-called synchronous vibration that is caused by unbalances or by circumferential periodical pressure field known as nozzle excitation. Then, blade vibration fre-

quencies are integer multiple of shaft rotation frequencies that coincide with some eigenfrequencies of a bladed disk. These critical speeds can be predicted in the design. In the latter case, the vibration is caused by aeroelastic coupling between blades and a flow field. According to distortions of flow and its volumetric rate around blade airfoil, the different types of self-excited vibration occur non-synchronously with respect to the rotation frequency. These states in full operational range are more difficult to predict. The bladed wheel with sufficient dissipation of mechanical energy is the protection against this case. Since the material damping of the blades (mostly of metal) is very low, it is necessary to increase the damping by additional construction damping. Therefore, dry friction damping as blade to blade or blade to ground with couplings in roots, shrouds or platforms is introduced into the turbine design (e.g. [1]). Besides very positive effect of higher damping on the self-excited vibration, it decreases forced response vibration level, too.

The influence of the friction damping [2] on the dynamic behaviour of the blading is a complex problem of continuum mechanics as to the dynamic behaviour of spatial distorted blades coupled by disk [3] and time-variant surface to surface dynamical contact with friction. It leads to multipoint non-Hertzian contacts influenced by production accuracy and roughness of the contact surfaces, thermo-mechanical coupling, etc [4]. There are many approaches that allow to solve this problem from analytical models with few degrees of freedom to numerical spatial 3D models [5–7].

Plenty of publications deal with the friction phenomena in blade dynamics and many design variants are used. A detailed investigation of influences of friction on dynamical response of a simplified mechanical system represented by a beam can be found in [8]. One of the design possibilities is the usage of underplatform (wedge) dampers [9]. A method for the calculation of static balance supposing an in-plane motion of the wedge dampers is developed in [10]. An analytical approach is described in [11], and a comparison of numerical simulation results with the results obtained by linearization is shown in [12]. The equivalent linearization method for the evaluation of friction effects in blade dynamics represented by a very simple discrete mechanical system is discussed in [13]. Some comparison of experimental and theoretical analysis is shown in [14], and pure experimental results are described in [15]. The possibilities of friction damping at turbine root joints are studied and numerically solved in [16].

Chosen recent developments of the methodology for spatial interaction of blades are shown in [17], where the multi-harmonic balance method and numerical integration approach are employed. A fully finite element solution is presented in [18]. Interaction of blades and their disk is studied in [19]. The general Coulomb law, where friction coefficient is a function of a relative velocity and quality of surfaces, is mostly used for the description of friction forces in contacts. It causes a nonlinear behaviour especially in non-stationary loading and macroslip motion in the contact. The friction model can be simplified for stationary harmonic vibration by an equivalent linearization of friction forces (the harmonic balance method) [20].

For the analysis of friction processes and their influence on blades' vibrations presented in this paper, the numerical modelling and experiments of the blade couple with the friction element made of steel or composite material with ARAMID fibres in non-rotating state were performed. The main attention herein is paid to the results with ARAMID material. This material has very good friction properties, wear and heat resistances that could sustain the heavy operational conditions of the steam turbine blades.

The paper is structured as follows. The experimental set-up and the results of measurements are described in the second chapter. As to the experiment, the excitation of one blade with both sweep sine and resonant by electromagnet was accomplished. Time characteristics of the excitation force, blade and friction element responses were measured for different normal pressures in the contact areas. The basic numerical model and the complex numerical model are described in the third and the fourth chapter, respectively. The fifth chapter is focused on the presentation of the numerical results, discussion and comparison with experimental results.

2 Experimental investigation of two blades vibration with ARAMID friction element

The experimental set-up is shown in Fig. 1. The blades (blade A, blade B—a prismatic part of blades has width 0.02 m and thickness 0.01 m, length 0.2 m, total length 0.25 m) were clamped into the steel block by bolts. The friction element (FE) (mass of 0.0084 kg) placed

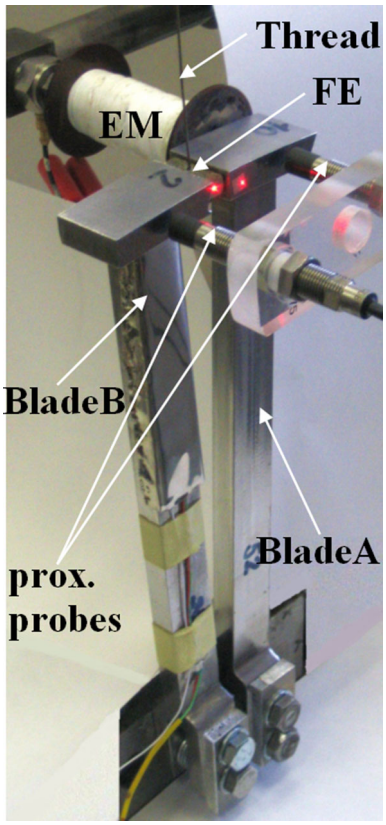

Fig. 1 Picture of the experimental set-up (*red spots*—target laser points). (Color figure online)

in the slot between the blade ends (height 0.01 m, mass 0.078 kg) was radially extruded by the thread pre-stressed by the static weight over the pulley (Fig. 1). The radial force was set in range $0.5 \div 2$ N. The excitation was performed by electromagnet (EM) acting to the blade A. The electromagnetic force was considered up to 1.8 N. The experimental set-up is shown in Fig. 2.

The displacements u_A resp. u_B of the each blade were picked up by the Schenk IN-081 proximity probes and at the same time the velocities v_A of the blade A and v_{ET} of the friction element by the POLYTEC laser vibrometers. The electromagnet was supplied by LDS power amplifier and controlled by signal y_E of the HP 33120A generator. Force f_{EM} of the electromagnet was measured by the B&K8200 force transducer. Time characteristics of the force, the blade and the friction element responses and the generator signal were registered in the YOKOGAWA DL750 Scope Recorder for different force levels and static pre-stresses of the friction element in the slot.

A short block of the harmonic excitation with resonant first flexural frequency 130.1 Hz generated by the electromagnet was employed in order to perform the friction coupling analysis. The time length of excitation was chosen to achieve a stationary resonant vibration. Then, the excitation was abruptly switched off. The damping effect was evaluated from vibration amplitude decay of blades after switching off the excitation. Damping ratios were identified from amplitude logarithmic decrement by Hilbert's transformation.

The typical results of the two blades vibration with the friction element are shown in the Figs. 3, 4 and 5

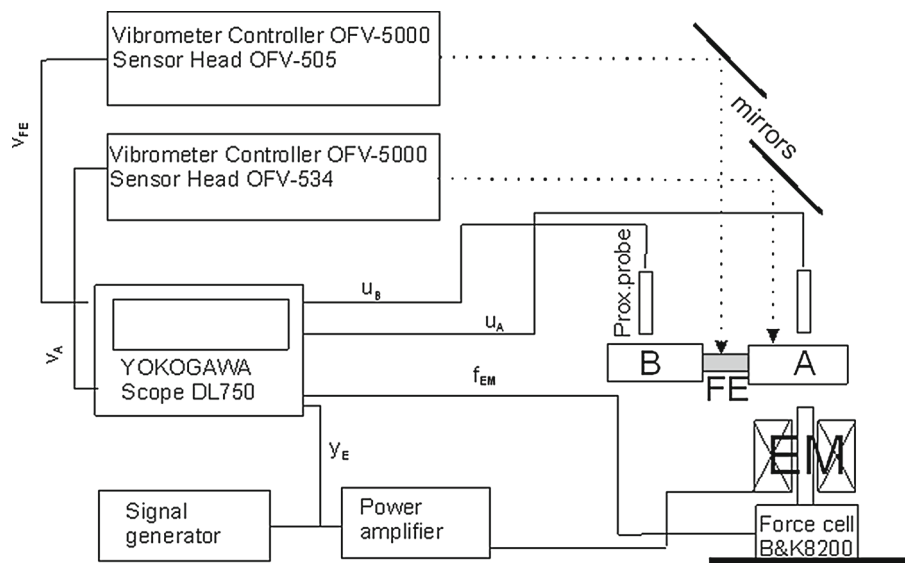

Fig. 2 Block scheme of the experimental set-up

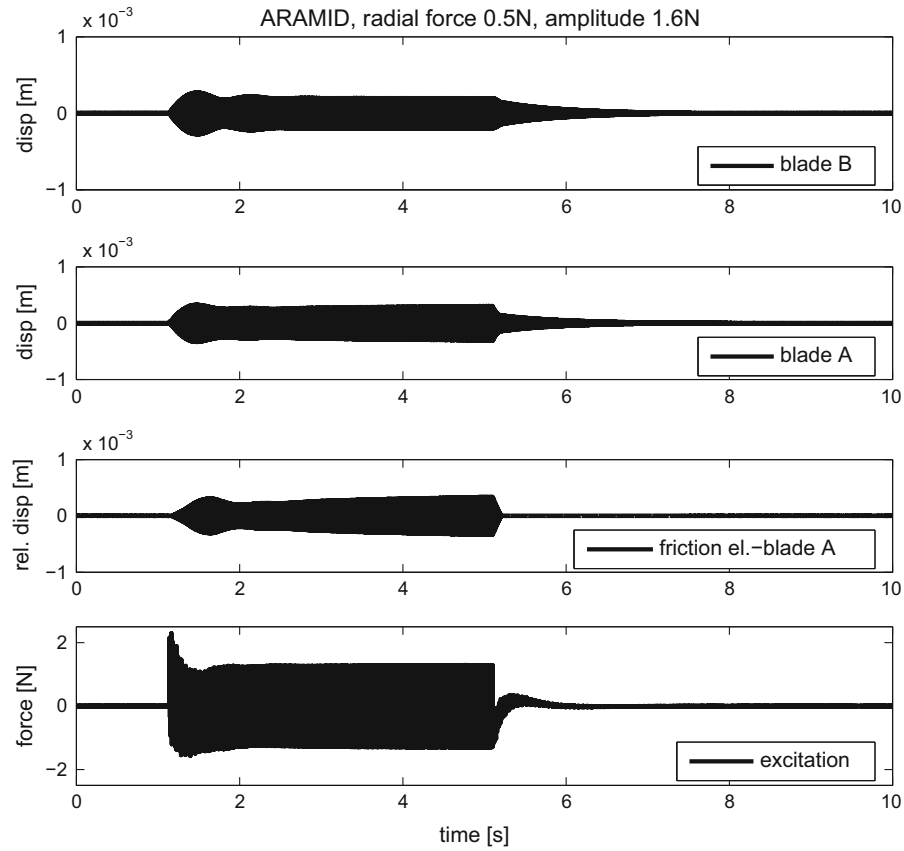

Fig. 3 Graphs of the case I: (*top*) displacements of the blades B and A, relative displacement of the friction element and electromagnet force; (*bottom*) displacement of the blade A with the amplitude envelope and damping ratio during the attenuation

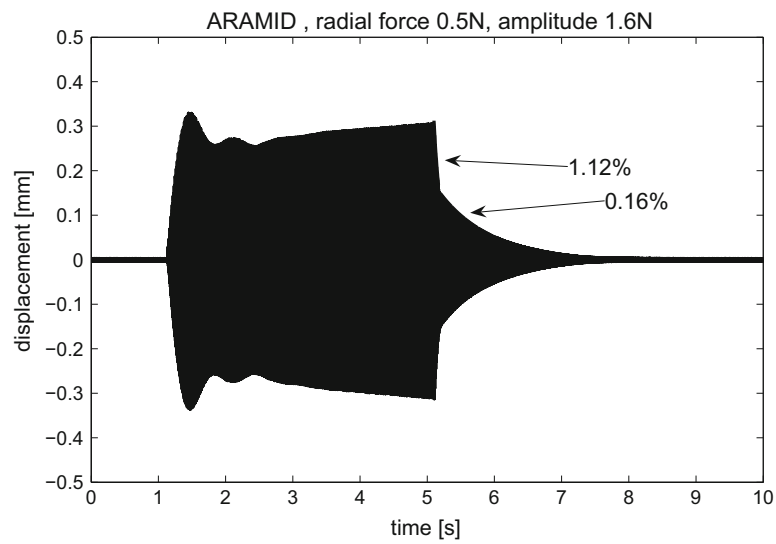

for three combinations (I–III) of the radial force F_r and excitation amplitude F_a values:

case I—$F_r = 0.5$ N, $F_a = 1.6$ N,
case II—$F_r = 1$ N, $F_a = 0.8$ N,
case III—$F_r = 1$ N, $F_a = 1.8$ N.

The top graphs of Figs. 3, 4 and 5 depict the measured signals, i.e. displacements of blades A, B, relative displacement of the friction element with respect to the

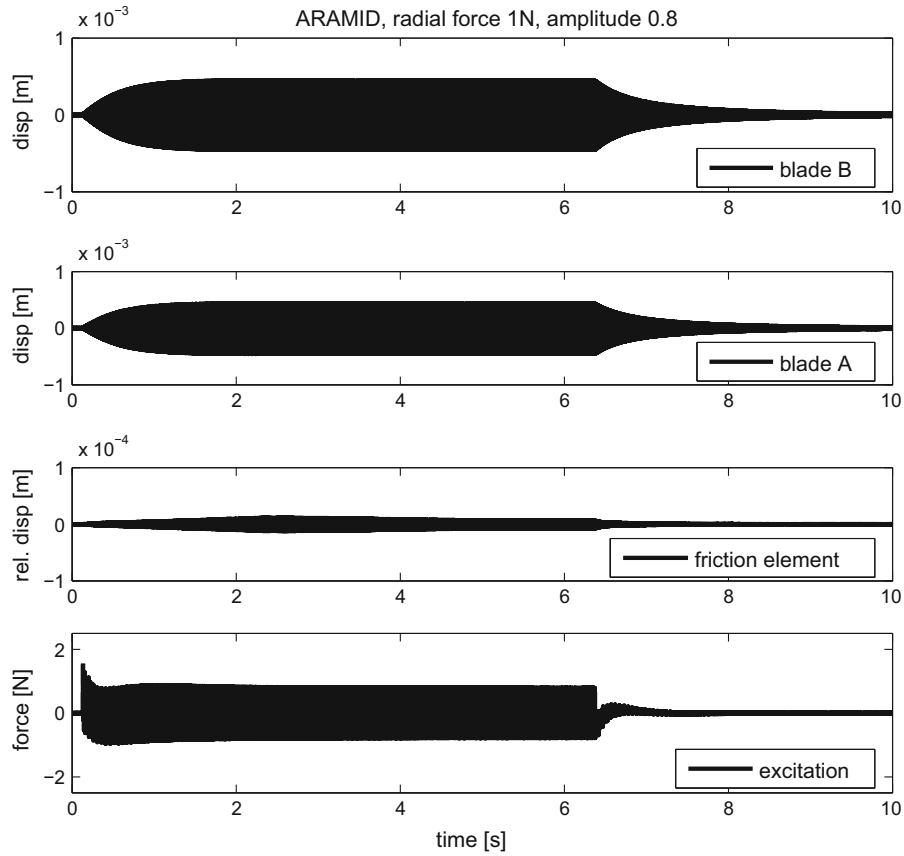

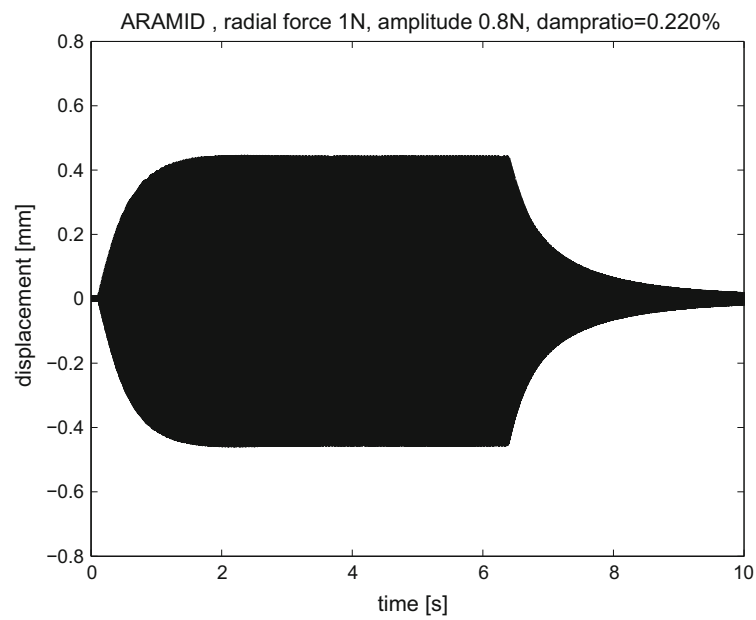

Fig. 4 Graphs of the case II: (*top*) displacements of the blades B and A, relative displacement of the friction element and electromagnet force; (*bottom*) displacement of the blade A with the amplitude envelope and damping ratio during the attenuation

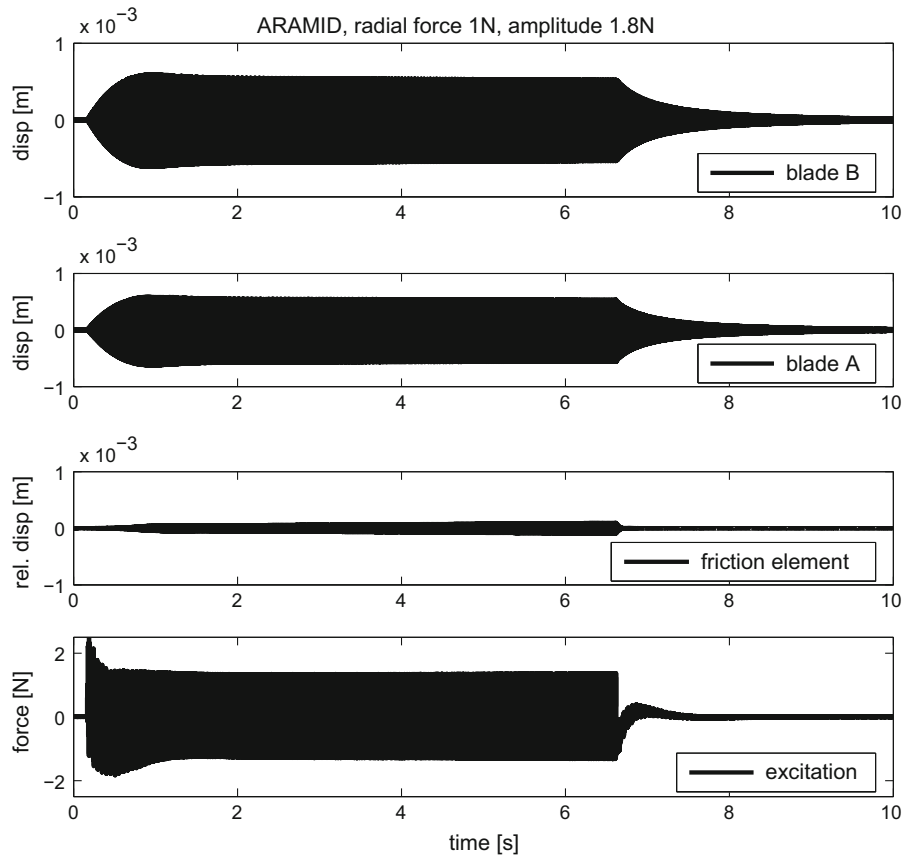

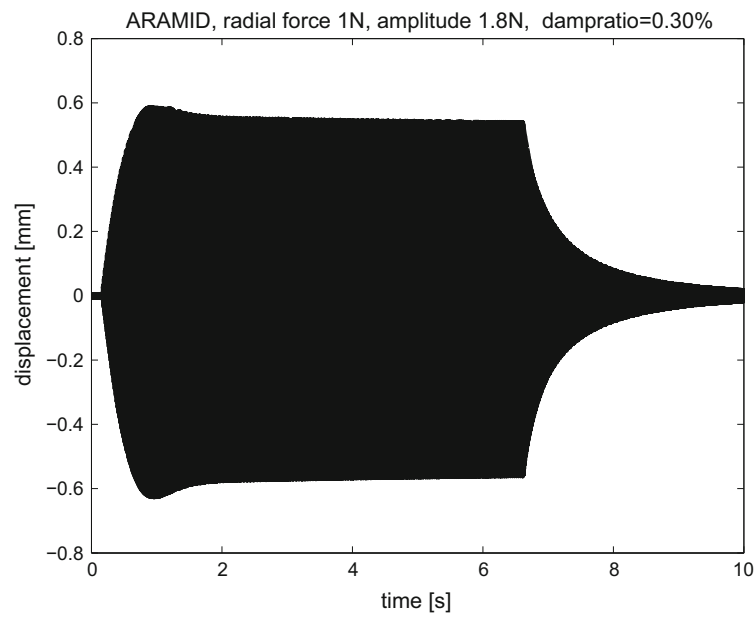

Fig. 5 Graphs of the case III: (*top*) displacements of the blades B and A, relative displacement of the friction element and electromagnet force; (*bottom*) displacement of the blade A with the amplitude envelope and damping ratio during the attenuation

blade A and electromagnet force f_{em}. The relative displacement was evaluated from the difference of velocities v_A and v_{ET} after their numerical integrations. The bottom graphs in Figs. 3, 4 and 5 depict the displacement of the Blade A with evaluated damping ratios at the attenuation after switching off of the electromagnet current supply.

Nonlinear effect of dry friction is mostly pronounced for the case I (Fig. 3). The relative displacement of the friction element shows macroslip (the first stage) and microslip (the second stage) movements of the friction element during the attenuation. Due to macroslips, the vibration amplitudes of the blades fall down with high damping ratio 1.12 % in the first stage. After the first stage, the macroslip movement transfers into the microslip movement of the friction element between the blades and the damping ratio drops to 0.16 %.

The weak effect of microslips on damping behaviour of the blade couple can be observed in case II (Fig. 4). The relative displacement of the friction element is in the range of approximately $\pm 10^{-5}$ m, and the damping rate is 0.2 %. The attenuation is almost exponential in the whole time.

The usage of the same radial force and a higher excitation force (case III, Fig. 5) causes higher excited amplitudes of blade vibration, higher relative displacement of the friction element and slightly higher damping ratio (0.3 %) of the attenuation.

Due to higher damping ratio in case I (Fig. 3), the vibration amplitudes of blades A, B are approximately half than their amplitudes in case II (Fig. 4), where the relative motion of the friction element is smaller due to higher radial force and higher adhesion forces between the friction element and the blades.

3 Simplified mathematical model of two blades coupling by friction element

The computational model of the couple of steel blades, which are clamped into the non-rotating disk, is shown in Fig. 6. The ends of the blades are fixed in end nodal points to the blade heads that are modelled as rigid bodies. The rigid friction element is pulled using the constant tension force F_C into a wedge gap between the blade heads. The second blade ($j = 2$) is excited in the head's centre of gravity parallel with the contact

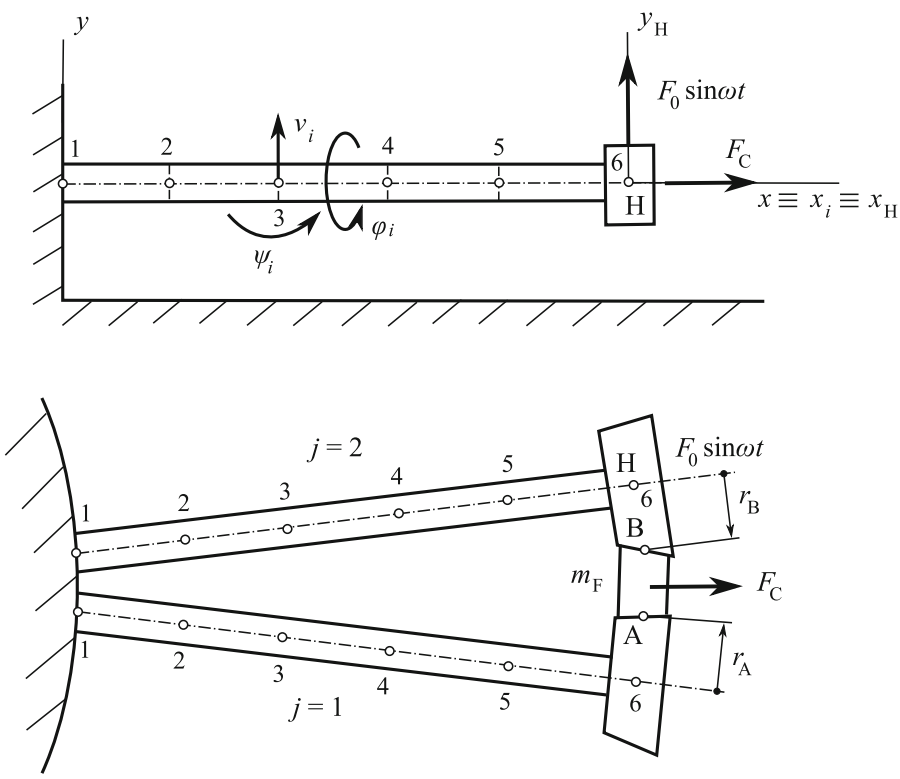

Fig. 6 Scheme of the couple of blades with the friction element—the basic model (the numbers denote finite element nodes)

surface (direction of y axis) by harmonic time-varying force $F_0 \sin \omega t$.

The blades have been discretized using the finite element method [21] by five identical beam elements with three degrees of freedom in every node i, transversal v_i, flexural ψ_i and torsional φ_i displacements from static state equilibrium. Mass $\mathbf{M}_e$ and stiffness $\mathbf{K}_e$ matrices of the beam element e between nodal points i and $i+1$ of length l have been derived in the configuration space

$$\mathbf{q}_e = [\, v_i \;\; \psi_i \;\; v_{i+1} \;\; \psi_{i+1} \;\; \varphi_i \;\; \varphi_{i+1} \,]^T \tag{1}$$

using identities

$$\frac{\partial E_k^{(e)}}{\partial \dot{\mathbf{q}}_e} = \mathbf{M}_e \dot{\mathbf{q}}_e, \quad \frac{\partial E_p^{(e)}}{\partial \mathbf{q}_e} = \mathbf{K}_e \mathbf{q}_e, \tag{2}$$

where $E_k^{(e)}$ is kinetic and $E_p^{(e)}$ potential (strain) energy of the beam element. The lateral deformations of the centreline beam element are approximated in the form

$$v(x,t) = \mathbf{v}(x)\mathbf{S}_1^{-1}\mathbf{q}_1^{(e)}(t) \tag{3}$$

and the torsional deformation in the form

$$\varphi(x,t) = \boldsymbol{\varphi}(x)\mathbf{S}_2^{-1}\mathbf{q}_2^{(e)}(t), \tag{4}$$

where

$$\mathbf{v}(x) = \begin{bmatrix} 1 & x & x^2 & x^3 \end{bmatrix}, \quad \boldsymbol{\varphi}(x) = [\, 1 \;\; x \,], \tag{5}$$

$$\mathbf{S}_1 = \begin{bmatrix} 1 & 0 & 0 & 0 \\ 0 & 1 & 0 & 0 \\ 1 & l & l^2 & l^3 \\ 0 & 1 & 2l & 3l^2 \end{bmatrix}, \quad \mathbf{S}_2 = \begin{bmatrix} 1 & 0 \\ 1 & l \end{bmatrix}, \tag{6}$$

and

$$\mathbf{q}_1^{(e)}(t) = [\, v_i \;\; \psi_i \;\; v_{i+1} \;\; \psi_{i+1} \,]^T, \mathbf{q}_2^{(e)}(t) = [\, \varphi_i \;\; \varphi_{i+1} \,]^T. \tag{7}$$

The beam element mass and stiffness matrices are of the form

$$\mathbf{M}^{(e)} = \varrho \begin{bmatrix} \mathbf{S}_1^{-T}(A\mathbf{I}_v + J_z\mathbf{I}_{v'})\mathbf{S}_1^{-1} & \mathbf{0} \\ \mathbf{0} & J_p\mathbf{S}_2^{-T}\mathbf{I}_\varphi\mathbf{S}_2^{-1} \end{bmatrix}, \tag{8}$$

$$\mathbf{K}^{(e)} = \varrho \begin{bmatrix} EJ_z\mathbf{S}_1^{-T}\mathbf{I}_{v''}\mathbf{S}_1^{-1} & \mathbf{0} \\ \mathbf{0} & GJ_k\mathbf{S}_2^{-T}\mathbf{I}_{\varphi'}\mathbf{S}_2^{-1} \end{bmatrix}, \tag{9}$$

where auxiliary integral matrices are

$$\mathbf{I}_v = \int_0^l \mathbf{v}^T(x)\mathbf{v}(x)\,\mathrm{d}x, \; \mathbf{I}_{v'} = \int_0^l \mathbf{v}'^T(x)\mathbf{v}'(x)\,\mathrm{d}x,$$
$$\mathbf{I}_{v''} = \int_0^l \mathbf{v}''^T(x)\mathbf{v}''(x)\,\mathrm{d}x,$$
$$\mathbf{I}_\varphi = \int_0^l \boldsymbol{\varphi}^T(x)\boldsymbol{\varphi}(x)\,\mathrm{d}x, \; \mathbf{I}_{\varphi'} = \int_0^l \boldsymbol{\varphi}'^T(x)\boldsymbol{\varphi}'(x)\,\mathrm{d}x. \tag{10}$$

Every beam element is determined by parameters φ (mass density), A (blade cross-section area), J_z (second moment of the blade cross-section area about the z-axis), J_p and J_k (polar and torsion resistance, second moment of the blade cross-section area), E (Young's modulus) and G (shear modulus) for particular blade material.

The configuration space (1) defined by vector $\mathbf{q}_e$ was created in order to efficiently derive the finite element matrices. The new configuration space

$$\widetilde{\mathbf{q}}_e = [\, v_i \;\; \psi_i \;\; \varphi_i \;\; v_{i+1} \;\; \psi_{i+1} \;\; \varphi_{i+1} \,]^T, \tag{11}$$

which is more suitable than (1) for the evaluation of blade dynamics results and for the manipulation with the model, will be used in further derivations. The simple coordinate transformation (transmutation) by means of matrix $\mathbf{P}$ can be written in the form

$$\mathbf{q}_e = \mathbf{P}\widetilde{\mathbf{q}}_e. \tag{12}$$

Transformed mass and stiffness matrices of the beam element are defined as

$$\widetilde{\mathbf{M}}_e = \mathbf{P}^T\mathbf{M}_e\mathbf{P}, \quad \widetilde{\mathbf{K}}_e = \mathbf{P}^T\mathbf{K}_e\mathbf{P}. \tag{13}$$

Using standard finite element procedures and after completion with blade mass matrices, we get the mass and stiffness matrices of blades

$$\mathbf{M}_j = \sum_{e=1}^{5} \mathrm{diag}\left(\mathbf{0},\; \widetilde{\mathbf{M}}_e,\; \mathbf{0}\right) + \mathbf{M}_H,$$
$$\mathbf{K}_j = \sum_{e=1}^{5} \mathrm{diag}\left(\mathbf{0},\; \widetilde{\mathbf{K}}_e,\; \mathbf{0}\right), \quad j = 1,\; 2. \tag{14}$$

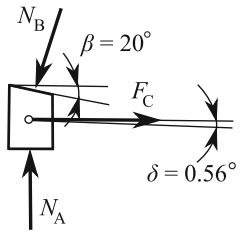

Fig. 7 Friction element pulled into a wedge gap between the blade shrouds—the basic model

in configuration space

$$\mathbf{q}_j = [\ldots\ v_i\ \psi_i\ \varphi_i\ \ \ldots]^T,\ i = 1,\ 2,\ \ldots,\ 5;\quad j = 1,\ 2. \tag{15}$$

The blade head is modelled in (14) by mass matrix

$$\mathbf{M}_H = \text{diag}\left(0,\ 0,\ \ldots,\ 0,\ m_H,\ I_{z_H},\ I_{x_H}\right) \in \mathbb{R}^{15,15} \tag{16}$$

determined by mass m_H and inertia mass moments I_{x_H}, I_{z_H} about x_H and z_H axes crossing the centre of head gravity H.

The friction element of mass m_F (see Fig. 7) is considered to be rigid body suspended on a thin elastic fibre with vertical stiffness k_F. The pulling force F_C represents centrifugal force. According to the blade couple and the friction element geometry (see Figs. 6, 7) the contact normal forces N_A and N_B, acting in contact areas between the friction element and blade shrouds, are calculated based on the static equilibrium conditions of the friction element in the form

$$N_A = F_C \frac{\cos(\beta + \delta)}{\sin\beta},\quad N_B = F_C \frac{\cos\delta}{\sin\beta}, \tag{17}$$

where δ is the angle between the radius vector of the friction element centre of gravity and the radial contact area of the first blade shroud.

The friction forces on contact areas, assuming vertical displacement v_F of the friction element, are approximated by continuous function depending on the slip velocity c_A or c_B

$$c_A = \dot{v}_6^{(1)} + r_A\dot{\varphi}_6^{(1)} - \dot{v}_F,\quad c_B = \dot{v}_6^{(2)} - r_B\dot{\varphi}_6^{(2)} - \dot{v}_F \tag{18}$$

of the central contact points A or B (Fig. 6). The characteristic of friction forces F_t is displayed in Fig. 8, where N is the normal force, f_s is the static (Coulomb) coefficient of friction, f_d is the dynamic coefficient of friction and d is the coefficient of friction decrease between maximal and minimal values. The characteristic respects microslips at very low slip velocities ($|c| \le c_k$). The resulting friction forces in contact areas are defined as

$$\begin{aligned} F_{tX} &= N_X[f_d + (f_s - f_d)\mathrm{e}^{-d(|c_X| - c_k)}]\text{sign}(c_X),\\ &\quad \text{for}\quad |c_X| > c_k,\\ F_{tX} &= N_X\frac{c_X}{c_k},\\ &\quad \text{for}\quad |c_X| \le c_k,\quad X = A,\ B. \end{aligned} \tag{19}$$

The critical slip velocity c_k defines the length of the interval in which the Coulomb friction discontinuity is approximated via a steep straight line (micro-slip phase).

The mathematical model of the whole system of a couple of blades with the friction element, assuming only dominant vertical displacement v_F of the friction element in a wedge gap, is of the form

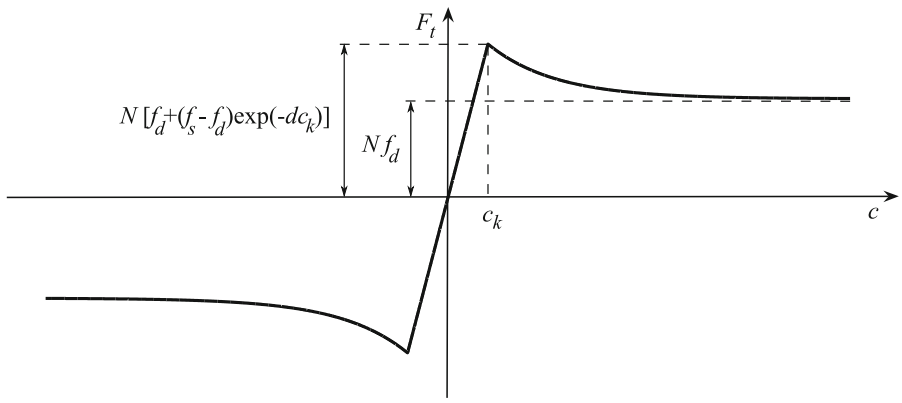

Fig. 8 Friction characteristics ($c \equiv c_A$ or $c \equiv c_B$)

$$\begin{bmatrix} \mathbf{M}_1 & \mathbf{0} & \mathbf{0} \\ \mathbf{0} & m_F & \mathbf{0} \\ \mathbf{0} & \mathbf{0} & \mathbf{M}_2 \end{bmatrix} \begin{bmatrix} \ddot{\mathbf{q}}_1 \\ \ddot{v}_F \\ \ddot{\mathbf{q}}_2 \end{bmatrix} + \begin{bmatrix} \mathbf{B}_1 & \mathbf{0} & \mathbf{0} \\ \mathbf{0} & 0 & \mathbf{0} \\ \mathbf{0} & \mathbf{0} & \mathbf{B}_2 \end{bmatrix} \begin{bmatrix} \dot{\mathbf{q}}_1 \\ \dot{v}_F \\ \dot{\mathbf{q}}_2 \end{bmatrix} + \begin{bmatrix} \mathbf{K}_1 & \mathbf{0} & \mathbf{0} \\ \mathbf{0} & k_F & \mathbf{0} \\ \mathbf{0} & \mathbf{0} & \mathbf{K}_2 \end{bmatrix} \begin{bmatrix} \mathbf{q}_1 \\ v_F \\ \mathbf{q}_2 \end{bmatrix} = \begin{bmatrix} \mathbf{0} \\ 0 \\ \mathbf{f}_2 \sin(\omega t) \end{bmatrix} + \begin{bmatrix} -\mathbf{f}_A(c_A) \\ F_{tA}(c_A) + F_{tB}(c_B) \\ -\mathbf{f}_B(c_B) \end{bmatrix}, \quad (20)$$

where $\mathbf{B}_j$, $j = 1, 2$ are matrices of the blade proportional damping. The harmonic excitation of the second blade is described by vector $\mathbf{f}_2 \sin(\omega t)$ with nonzero 13th coordinate $F_0 \sin(\omega t)$. Vectors $\boldsymbol{f}_X$, $X = A,\ B$, expressing friction effects in the contact points A, B of the blade heads, are of the form

$$\mathbf{f}_A(c_A) = F_{tA}[0\,0\,\ldots\,1\,0\,r_A\,]^T \in \mathbb{R}^{(15)},$$
$$\mathbf{f}_A(c_B) = F_{tB}[0\,0\,\ldots\,1\,0\,-r_B\,]^T \in \mathbb{R}^{(15)}, \quad (21)$$

where constants r_A, r_B are perpendicular distances between the contact points and the axis of the blades (see Fig. 6).

4 Complex mathematical model

The usage of the simplified mathematical model described in the previous chapter can be advantageous in case of basic problems concerning the structural complexity and the complexity of excitation. The more complex model (Fig. 9) utilizable for more structurally complex cases will be shown in this chapter. Moreover, the complex blade couple model will be derived considering all effects of a disk rotation for sake of later usage

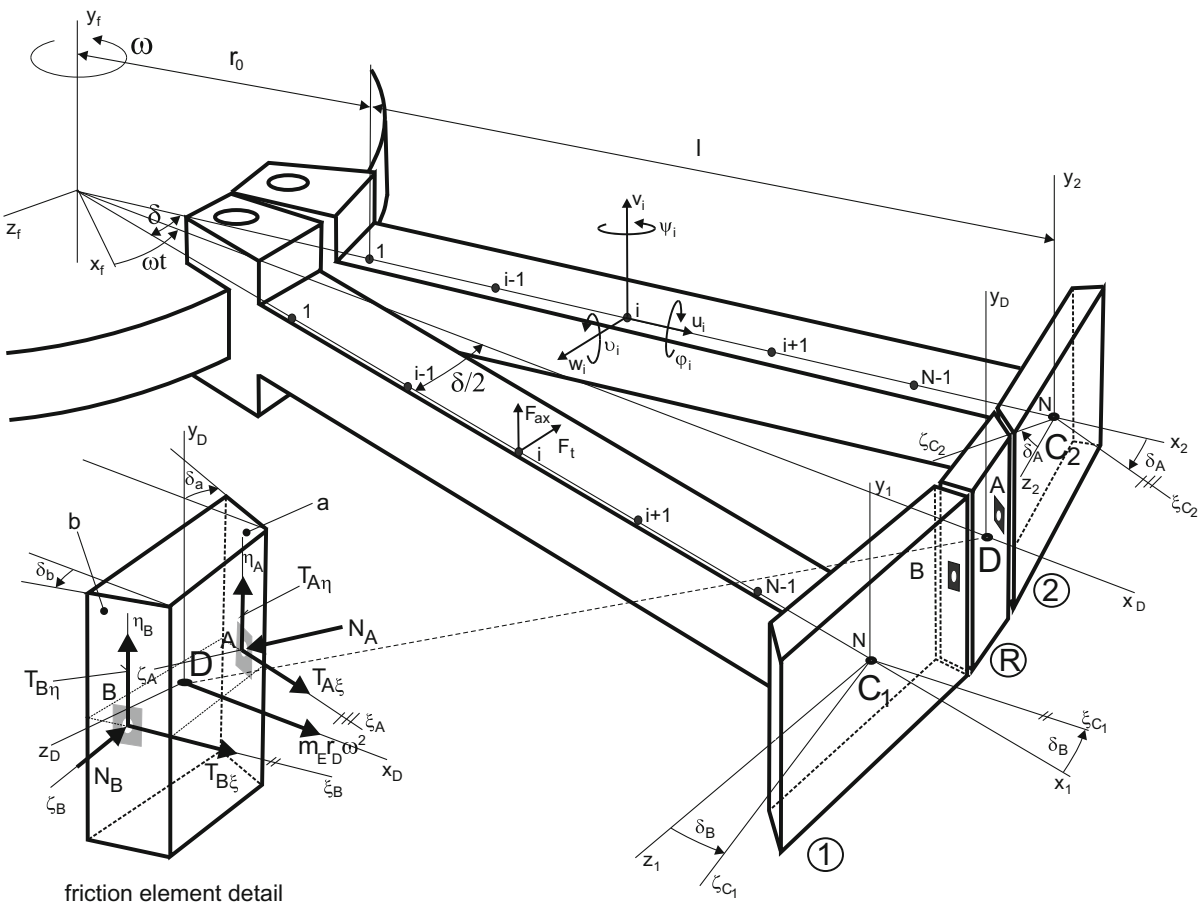

Fig. 9 Scheme of the couple of blades with the friction element and its detail—the complex model

in the general problems of bladed disk dynamics. The review of various modelling methodologies for rotating blade dynamics can be found, e.g. in [22] or [23].

As a simplification, the contacts of the friction element and the blade shrouds (see Fig. 9) are concentrated to the rectangular effective area with geometric centre in point B (in plane b defined by axes $\xi_B \eta_B$) and to the rectangular effective area with geometric centre in point A (in plane a defined by axes $\xi_A \eta_A$), respectively. The blades are modelled as 1D continuum discretized by beam finite elements with uniformly distributed nodes at axes of the blades. The first nodes of the blades are fixed to the rigid frame rotating with angular velocity ω. End nodes C_1 and C_2 of the blades are fixed to the blade shrouds modelled as rigid bodies because the shrouds are obviously stiffer then the blades. The spatial motion of all blade nodes as well as the friction element is characterized by six degrees of freedom. As the blades rotate, the centrifugal force $m_E r_D \omega^2$ pushes the friction element towards contact surfaces a and b of the adjacent blade shroud. In case of numerical simulation of the experimental measurement, the centrifugal force will be substituted by the proper constant force.

The friction element acts on the blades by contact normal forces N_X and contact torques $M_{\xi_X}, M_{\eta_X}, X = A, B$ and by friction forces $\overrightarrow{T}_X(T_{X\xi}, T_{X\eta})$ and friction torques $M_{\zeta_X}, X = A, B$ in contact surfaces.

The real excitation in turbines can be defined as harmonic forces with the nozzle passing frequency (i.e. the first engine order times number of nozzles) acting in tangential (F_t) and axial (F_{ax} parallel to axis of rotation) direction. Excitation forces can be uniformly concentrated in nodes along the blades. The choice of excitation type is general, and it does not influence the modelling approach. However, the excitation forces in this paper will be limited to the single force in y-direction in order to simulate the same conditions as in the experimental set-up.

Equations of motion of the blades with the shroud and the friction element can be expressed in rotating local coordinate systems x_j, y_j, z_j, $j = 1, 2$ (the blades) and x_D, y_D, z_D (the friction element), where axes x_j are the axes of the blades, and axis x_D corresponds to the radial direction from the disk centre to the friction element. Axes y_j, y_D are parallel to the fixed axis of disk rotation y_f (see Fig. 9). The vectors of nodal blade generalized coordinates

$$\mathbf{q}_j = [\ldots u_i, v_i, w_i, \varphi_i, \vartheta_i, \psi_i, \ldots]_j^T, \quad j = 1, 2, \tag{22}$$

are expressed by translational displacements and rotational displacements in nodes $i = 1, \ldots, N$ of the blade j. The equations of motion of two blades with shroud and without the friction element are of the form (see e.g. [24])

$$\mathbf{M}_B \ddot{\mathbf{q}}_j + (\omega \mathbf{G}_B + \mathbf{B}_B)\dot{\mathbf{q}}_j + (\mathbf{K}_{s,B} - \omega^2 \mathbf{K}_{d,B} + \omega^2 \mathbf{K}_{\omega,B})\mathbf{q}_j = \mathbf{f}_{\omega,B} + \mathbf{f}_{Bj}(t), \tag{23}$$

where symmetric matrices of order $6N$ $\mathbf{M}_B, \mathbf{B}_B, \mathbf{K}_{s,B}$, $\mathbf{K}_{d,B}, \mathbf{K}_{\omega,B}$ are mass, material damping, static stiffness, softening under rotation and bending stiffening under rotation, respectively. The symmetrical matrix $\omega \mathbf{G}_B$ considers gyroscopic effects. Constant centrifugal forces are expressed by vector $\mathbf{f}_{\omega,B}$ and general time-dependent forces are expressed by vector $\mathbf{f}_{Bj}(t)$.

The spatial motion of the rigid friction element is described in rotating coordinate system x_D, y_D, z_D by generalized coordinates $\mathbf{q}_E = [u, v, w, \varphi, \vartheta, \psi]^T$, and the equations of motion of still isolated rigid friction element can be written in matrix form analogous to the blade model

$$\mathbf{M}_E \ddot{\mathbf{q}}_E + \omega \mathbf{G}_E \dot{\mathbf{q}}_E - \omega^2 \mathbf{K}_{d,E} \mathbf{q}_E = \mathbf{f}_{\omega,E}. \tag{24}$$

After placing the friction element in between the blade shroud, acting of contact elastic and friction forces is concentrated into contact points A and B.

Using configuration space of generalized coordinates defined by vector

$$\mathbf{q} = [\,\mathbf{q}_1^T,\ \mathbf{q}_E^T,\ \mathbf{q}_2^T\,]^T, \tag{25}$$

equation of motion of the whole system is written in the form

$$\mathbf{M}\ddot{\mathbf{q}} + (\omega \mathbf{G} + \mathbf{B} + \mathbf{B}_C)\dot{\mathbf{q}} + (\mathbf{K}_s - \omega^2 \mathbf{K}_d + \omega^2 \mathbf{K}_\omega + \mathbf{K}_C)\mathbf{q} = \mathbf{h}(\dot{\mathbf{q}}, \mathbf{q}) + \mathbf{f}(t). \tag{26}$$

In accordance with the equations of motion (23) and (24), the matrices stated below have block-diagonal structure

$$\mathbf{M} = \mathrm{diag}\,(\mathbf{M}_B,\ \mathbf{M}_E,\ \mathbf{M}_B)\,,$$
$$\mathbf{G} = \mathrm{diag}\,(\mathbf{G}_B,\ \mathbf{G}_E,\ \mathbf{G}_B)\,,$$

$$\mathbf{B} = \mathrm{diag}\,(\mathbf{B}_B,\ \mathbf{0},\ \mathbf{B}_B)\,,$$
$$\mathbf{K}_s = \mathrm{diag}\,\left(\mathbf{K}_{s,B},\ \mathbf{0},\ \mathbf{K}_{s,B}\right),$$
$$\mathbf{K}_d = \mathrm{diag}\,\left(\mathbf{K}_{d,B},\ \mathbf{K}_{d,E},\ \mathbf{K}_{d,B}\right),$$
$$\mathbf{K}_\omega = \mathrm{diag}\,\left(\mathbf{K}_{\omega,B},\ \mathbf{0},\ \mathbf{K}_{\omega,B}\right). \tag{27}$$

The influence of contact viscous-elastic and friction forces in (26) is represented by stiffness coupling matrix $\mathbf{K}_C$, damping matrix $\mathbf{B}_C$ comprising the influence of contact damping in contact surfaces and by vector $\mathbf{h}(\dot{\mathbf{q}}, \mathbf{q})$, which expresses nonlinear friction forces in friction couplings between the shroud of blade 1 and 2 and the friction element, respectively. Vector $\mathbf{h}(\dot{\mathbf{q}}, \mathbf{q})$ of nonlinear friction forces and torques can be expressed as

$$\mathbf{h}(\dot{\mathbf{q}}, \mathbf{q}) = \begin{bmatrix} \mathbf{0} \\ \vdots \\ \mathbf{0} \\ \mathbf{f}_1 \\ \mathbf{m}_1^F + \mathbf{m}_1 \\ \mathbf{f}_a + \mathbf{f}_b \\ \mathbf{m}_a^F + \mathbf{m}_b^F + \mathbf{m}_b + \mathbf{m}_a \\ \mathbf{0} \\ \vdots \\ \mathbf{0} \\ \mathbf{f}_2 \\ \mathbf{m}_2^F + \mathbf{m}_2 \end{bmatrix}, \tag{28}$$

where nonzero force and torque vectors are on the positions corresponding to the generalized coordinates of the blade shrouds and to the generalized coordinates of the friction element. For example, vector

$$\mathbf{f}_1 = [-T_{B\xi}\cos\delta_B,\ -T_{B\eta},\ T_{B\xi}\sin\delta_B]^T \tag{29}$$

and vector $\mathbf{m}_1^F$ express the effects of friction forces between the friction element and the shrouds on motion of the shroud of the first blade (see Fig. 9). Vector $\mathbf{m}_1$ expresses the effect of friction torque in case of relative rotation of two surfaces in contact. It is analogous for other vectors.

The contact stiffness matrix $\mathbf{K}_C$ can be linearized for constant normal forces $N_{X,0}$ $(X = A, B)$. These forces are calculated from static equilibrium condition of friction element

$$N_{X,0} = F_r \frac{\cos\delta_X}{\sin(\delta_a + \delta_b)}, \quad X = A, B, \tag{30}$$

where $F_r = m_E r_E \omega^2$ in case of rotation or F_r can be chosen according to the experimental set-up. Angles of contact surfaces skewing between blade shroud and friction element are displayed in Fig. 9. The contact stiffness matrix $\mathbf{K}_C$ connecting the blades with the friction element can be calculated based on the coupling (deformation) energy

$$E_C = \frac{1}{2}\sum_{\substack{X=A,B \\ i=1,2}} \mathbf{d}_{X,C_i}^T \mathbf{K}_X \mathbf{d}_{X,C_i},$$
$$\mathbf{d}_{X,C_i} = \mathbf{T}_{X,C_i}\mathbf{q}_{C_i} - \mathbf{T}_{X,E}\mathbf{q}_E, \tag{31}$$

where $\mathbf{q}_{C_i}$, $i = 1, 2$ are the vectors of generalized displacements in the last nodes C_i of blades, and $\mathbf{q}_E$ is the vector of friction element displacements. Matrices $\mathbf{T}_{X,C_i}$ and $\mathbf{T}_{X,E}$ in (31) transform the vectors of displacements of nodes C_i and D into displacements of contact points A, B on corresponding body in coordinate systems ξ_X, η_X, ζ_X. Diagonal local contact stiffness matrix

$$\mathbf{K}_X = \mathrm{diag}\left(0\ 0\ k_{\zeta_X}\ k_{\xi_X\xi_X}\ k_{\eta_X\eta_X}\ 0\right),\ (X = A, B) \tag{32}$$

in coordinate system ξ_X, η_X, ζ_X $(X = A, B)$ is defined by contact stiffness k_{ζ_X} in normal direction ζ_X to contact area and two rotational (flexural) stiffnesses $k_{\xi_X\xi_X}$, $k_{\eta_X\eta_X}$ about axes ξ_X and η_X (see Fig. 9).

The contact normal stiffnesses can be linearized for contact normal forces (30) according to

$$k_{\xi_X} = \frac{N_{X,0}}{\gamma_X},\ \gamma_X = c\sigma_X^p,\ \sigma_X = \frac{N_{X,0}}{A_{ef,X}},\ X = A, B, \tag{33}$$

where γ_X designates contact normal deformations, σ_X average contact pressure acting on effective are $A_{ef,X}$. Contact deformation coefficient c and contact exponent p were estimated using data published in [25]. The rotational stiffnesses were calculated based on the assumption of identical area contact stiffness $k_{\xi_X}/A_{ef,X}$ in an arbitrary point of effective contact area.

Contact stiffness matrix $\mathbf{K}_C$ was derived using identity

$$\frac{\partial E_C}{\partial \mathbf{q}} = \mathbf{K}_C\mathbf{q} \tag{34}$$

and contact damping matrix $\mathbf{B}_C$ in (26) was considered as proportional $\mathbf{B}_C = \beta \mathbf{K}_C$.

Model (26) can be solved by various mathematical methods with respect to the character of expected results. The most direct one is a numerical integration of nonlinear equations of motion, which will be used in the next chapter. The resulting variables are obtained for particular case in the form of time series, while all types of nonlinearities including complex excitation can be considered. Nevertheless, other valuable results can be obtained from an analysis based on more qualitative comparisons, which is, e.g. eigenvalue analysis or steady state harmonic analysis, see, e.g. [26].

5 Discussion and results comparison

The above-mentioned mathematical models of the blade couple with the friction element were implemented as an in-house software in the MATLAB system. The values of model parameters were set in accordance with the experimental set-up. All three cases (I–III) were numerically simulated by means of both basic and complex models using numerical integration of the nonlinear equations of motion (20) and (26). Material damping of the blades was considered 0.2 % for all eigenmodes in all simulated cases. The particular values of the friction model parameters were estimated on the basis of previous experimental results ($f_s = 0.6$, $f_d = 0.3$, $d = 2$, $c_k = 10^{-3}\,\mathrm{ms}^{-1}$).

The displacements of the blade A calculated by the basic model are shown in Figs. 10, 11 and 12. The displacements of the blade A calculated by the complex model are shown in Figs. 13, 14 and 15. The summary of evaluated damping ratios for all cases is in Table 1. The damping ratios for both experimental and numerical results were calculated from the particular parts of time history by means of an amplitude logarithmic decrement by Hilbert's transformation.

The course of the time histories in case I (Figs. 3, 10, 13) compared to the cases II and III is characterized by macroslip movements in the first stage of the vibration attenuation and by microslip movements in the second stage of the attenuation. It was an expected result since the amplitude value of the harmonic excitation force was relatively high, and the radial force value was lower comparing to other cases. Thus, the adhesion forces in the contact were exceeded, and the macroslip movements were induced.

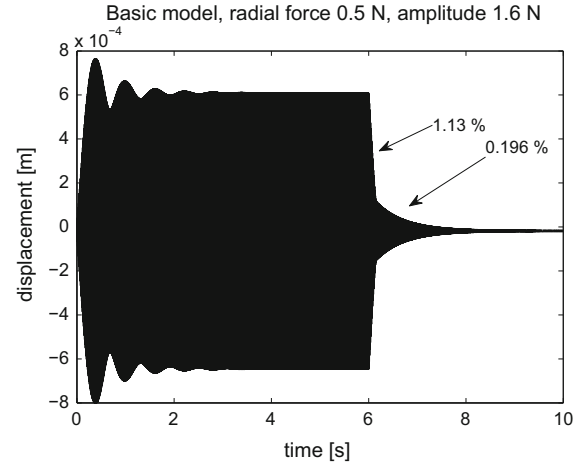

Fig. 10 Displacement of the blade A calculated using the basic model (case I)

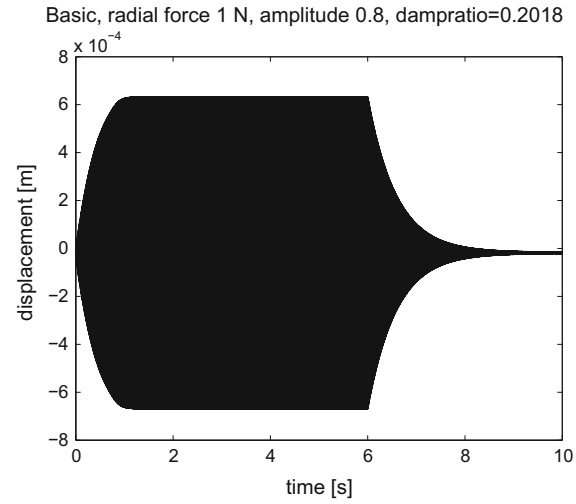

Fig. 11 Displacement of the blade A calculated using the basic model (case II)

The computed displacement amplitudes (Figs. 10, 13) are about twice higher compared to the experiment (Fig. 3). It is caused by the slight different eigenfrequencies of the real mechanical system and the numerical model of the system. The first bending eigenfrequency was calculated by the numerical model, and this value was used for the definition of the excitation frequency. If the same excitation frequency is used for the loading of the real mechanical system with slightly different bending eigenfrequency, the response will not be the same, i.e. the exact resonance is not achieved. The difference in the computed and measured ampli-

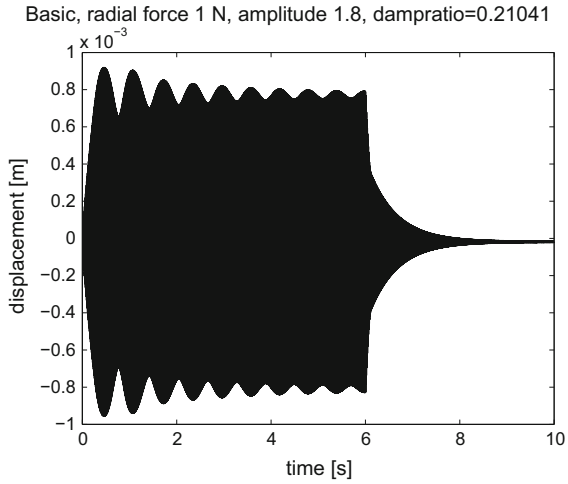

Fig. 12 Displacement of the blade A calculated using the basic model (case III)

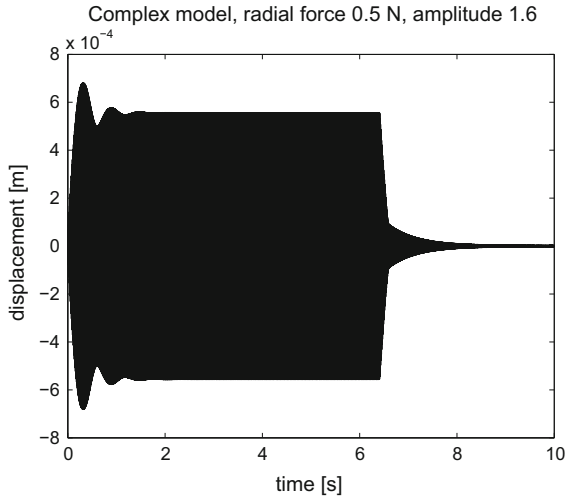

Fig. 13 Displacement of the blade A calculated using the complex model (case I)

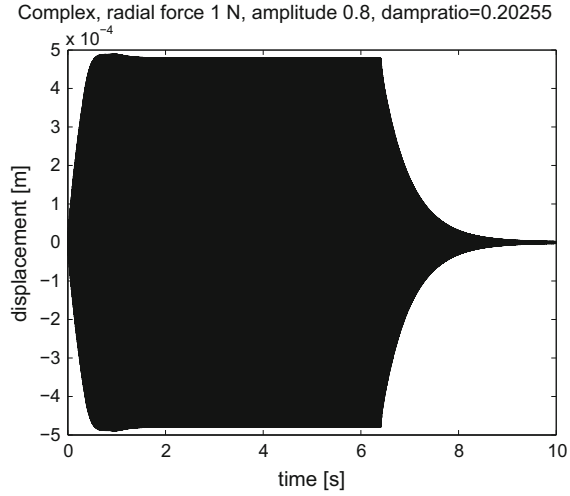

Fig. 14 Displacement of the blade A calculated using the complex model (case II)

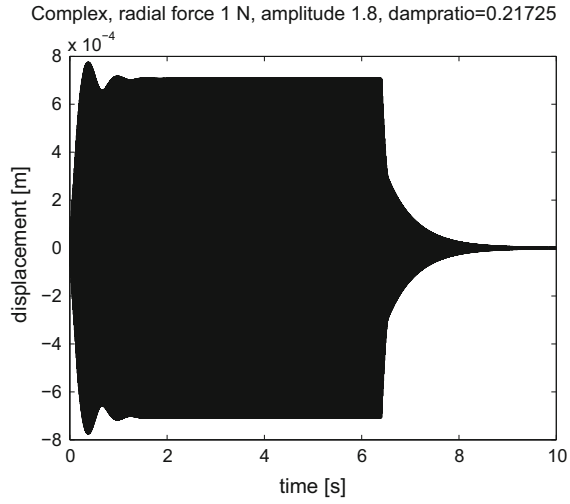

Fig. 15 Displacement of the blade A calculated using the complex model (case III)

tudes can be also caused by the fact that the excitation force has an ideal harmonic character in case of calculations, but this is not true for the real force generated by the electromagnet. Therefore, the larger resonance is obtained during the numerical simulation than during the experiment.

The course of the time history in case II (Figs. 4, 11, 14) is characterized by microslip movements in the whole attenuation region. It is caused by the small amplitude value of the electromagnet excitation force with respect to the radial extruding force. It should be noted that the situation is the same as in a real turbine in case of a low dynamic excitation of blades, which are locked for higher angular velocities (i.e. higher centrifugal forces acting on the friction element). The positive effect of the friction element placed in shrouding should occur in case of higher undesirable excitation (and successive higher vibration amplitudes of blades).

The accordance of the results obtained for case III (Figs. 5, 12, 15) is not so good as in the two previous cases. The measured course of the displacement time history for the blade A does not show a substantial transition between macroslip and microslip move-

Table 1 Evaluated damping ratios (%) for the experiment and both numerical models

	Case I	Case II	Case III
Experiment	1.120/0.160	0.220	0.300
Basic model	1.130/0.196	0.202	0.210
Complex model	1.019/0.224	0.203	0.217

ments. It is rather characterized by certain average switching between these two types of movements. On the other hand, the comparable numerical results show the standard macroslip movements in the first stage of the vibration attenuation and the microslip movements in the second stage of the attenuation (the damping ratios written in Table 1 are identified for the second stage). The inconsistency of the measured and calculated results in this limit case could be explained by insufficient friction model parameters, which are not suitable for the particular combination of the radial and transverse excitation forces.

6 Conclusions

The results of the experimental and numerical models of the dissipative effect of the friction elements inserted between the blade heads (and thus possibly creating a continuous shroud) are presented in the paper. The experimental stand consisting of two blades and one friction element was used for the obtaining of measured dynamic responses. Two numerical models such as the basic one and the complex one describing plane and spatial motion of the mechanical system, respectively, based on the finite element method and force description of bodies interaction were elaborated. The damping ratios evaluated from the blade vibration attenuations under different radial forces were chosen as a quantity to ascertain the dissipative effect of the proposed friction coupling. A satisfactory agreement between numerical results and experimental results, both for the case of macroslips and for the case of microslips in the contact areas, were reached.

As to the effectiveness of the dry friction damping, the high damping of blades is apparent after exceeding the adhesion forces and achieving the macroslip motion in the contact areas. A nonlinear effect in the vibration attenuation caused by the macroslip motion is mostly pronounced for this case. This motion transfers into the microslip motion with much lower damping after the decreasing of vibration amplitudes. Although the applied friction characteristic contains a part of the decreasing dependence of a friction force on relative velocity that can cause instability and self-excited oscillations at the constant velocity, due to the harmonic variation of the velocity, no self-excitation appeared in our investigations.

Mutual friction has positive effects concerning vibration suppression when the normal forces are under certain limit for given excitation (radial and axial forces). The amount of normal forces is determined by the shape (i.e. geometrical parameters) of the friction element and the sides of blade heads. One of the most important results of the work presented in this paper is that the developed modelling and simulation methodology can be used together with optimization tools in order to find the optimal shape of friction for chosen operation conditions of real bladed disks. The second significance of the paper is in the experimental and numerical verification of the friction element effects on vibration suppression.

Acknowledgments The work presented in this paper was supported by the research Project No. 101/09/1166 “Research of dynamic behaviour and optimization of complex rotating systems with nonlinear couplings and high damping materials” of Czech Science Foundation.

References

1. Sextro, W.: Dynamical Contact Problems with Friction. Springer, Berlin (2007)
2. Fang, J., Wang, Q., Wang, S., Wang, Q.: Min-max criterion to the optimal design of vibration absorber in a system with Coulomb friction and viscous damping. Nonlinear Dyn. (2012). doi:10.1007/s11071-012-0462-7
3. Rao, J.S.: Turbomachine Blade Vibration. Wiley Eastern Limited, New Delhi (1991)
4. Awrejcewicz, J., Pyr’yev, Y.: Nonsmooth Dynamics of Contacting Thermoelastic Bodies. Springer, Berlin (2009)
5. Pešek, L., Půst, L.: Influence of dry friction damping on bladed disk vibration. In: Náprstek, J., Horáček, J. (eds.) Vibration Problems ICOVP 2011, pp. 557–564. Springer, Berlin (2011)
6. Pešek, L., Půst, L.: Mathematical model of a blade couple connected by damping element. In: Roeck, G., Degrande, G., Lombaert, G., Muller, G. (eds.) Proceedings of 8th International Conference on Structural Dynamics, EURODYN2011, pp. 2006–2011. KU Leuven, Leuven (2011)
7. Voldřich, J.: Modelling of the three-dimensional friction contact of vibrating elastic bodies with rough surfaces. Appl. Comput. Mech. **3**, 241–252 (2009)
8. Cigeroglu, E., An, N., Menq, C.H.: A microslip friction model with normal load variation induced by normal motion. Nonlinear Dyn. **50**, 609–626 (2007)

9. Panning, L., Sextro, W., Popp, K.: Spatial dynamics of tuned and mistuned bladed disks with cylindrical and wedge-shaped friction dampers. Int. J. Rotating Mach. **9**, 219–228 (2003)
10. Firrone, C.M., Zucca, S.: Underplatform dampers for turbine blades: The effect of damper static balance on the blade dynamics. Mech. Res. Commun. **36**, 515–522 (2009)
11. Borrajo, J.M., Zucca, S., Gola, M.M.: Analytical formulation of the Jacobian matrix for non-linear calculation of forced response of turbine blade assemblies with wedge friction dampers. Int. J. Non-Linear Mech. **41**, 1118–1127 (2006)
12. Csaba, G.: Forced response analysis in time and frequency domains of a tuned bladed disk with friction dampers. J. Sound Vib. **214**, 395–412 (1998)
13. Cha, D., Sinha, A.: Statistics of responses of a mistuned and frictionally damped bladed disk assembly subjected to white noise and narrow band excitations. Probab. Eng. Mech. **21**, 384–396 (2006)
14. Toufine, A., Barrau, J., Berthillier, M.: Dynamics study of a structure with flexion-torsion coupling in the presence of dry friction. Nonlinear Dyn **18**, 321–337 (1999)
15. Tokar, I.G., Zinkovskii, A.P., Matveev, V.V.: On the problem of improvement of the damping ability of rotor blades of contemporary gas-turbine engines. Strength Mater. **35**, 368–375 (2003)
16. Zucca, S., Firrone, C.M., Gola, M.M.: Numerical assessment of friction damping at turbine blade root joints by simultaneous calculation of the static and dynamic contact loads. Nonlinear Dyn. **67**, 1943–1955 (2012)
17. Gu, W., Xu, Z., Wang, S.: Advanced modelling of frictional contact in three-dimensional motion when analysing the forced response of a shrouded blade. Proc. IMechE, Part A: J. Power. Energy **224**, 573–582 (2010)
18. Bachschmid, N., Bistolfi, S., Ferrante, M., Pennacchi, P., Pesatori, E., Sanvito, M.: An investigation on the dynamic behaviour of blades coupled by shroud contacts. In: Proceedings of SIRM 2011. Darmstadt, Germany (2011)
19. Petrov, E.P., Ewins, D.J.: Effects of damping and varying contact area at blade-disk joints in forced response analysis of bladed disk assemblies. J. Turbomach. **128**, 403–410 (2006)
20. Pešek, L., Půst, L., Vaněk, F., Veselý, J.: FE modeling of blade couple with friction contacts under dynamic loading. In: Proceedings of 13th World Congress in Mechanism and Machine Science 2011. IFToMM, Guanajuato, Mexico (2011)
21. Byrtus, M., Hajžman, M., Zeman, V.: Dynamics of rotating systems. University of West Bohemia, Pilsen (2010) (in Czech)
22. Lacarbonara, W., Arvin, H., Bakhtiari-Nejad, F.: A geometrically exact approach to the overall dynamics of elastic rotating blades–part 1: linear modal properties. Nonlinear Dyn. (2012). doi:10.1007/s11071-012-0486-z
23. Yao, M.H., Chen, Y.P., Zhang, W.: Nonlinear vibrations of blade with varying rotating speed. Nonlinear Dyn. (2012). doi:10.1007/s11071-011-0231-z
24. Kellner, J.: Vibrations of turbine blades and bladed disks. PhD Thesis. University of West Bohemia, Pilsen, in Czech (2009)
25. Rivin, E.I.: Stiffness and Damping in Mechanical Design. Marcel Dekker, New York (1989)
26. Zeman, V., Byrtus, M., Hajžman, M.: Harmonic forced vibration of two rotating blades with friction damping. Eng. Mech. **17**, 187–200 (2010)